scientific reports

Check for updates

OPEN

Inversely polarized thermo-electrochemical power generation via the reaction of an organic redox couple on a TiO_2/Ti mesh electrode

Hiroto Eguchi[1], Takashi Kobayashi[2], Teppei Yamada[2,3]✉, David S. Rivera Rocabado[4], Takayoshi Ishimoto[4,5]✉ & Miho Yamauchi[1,6,7]✉

We demonstrate thermo-electrochemical (TEC) conversion using a biocompatible redox couple of lactic acid and pyruvic acid on earth-abundant TiO_2. The TEC cell exhibited a positive Seebeck coefficient of 1.40 mV K^{-1}. DFT calculations figured out that the adsorption of intermediate species and protons on TiO_2 controls both the redox reaction and current polarity.

The thermoelectric conversion is a powerful tool to upgrade widely distributed low-grade heat energies, which are characterized by temperatures lower than 200 °C, such as waste heat, geothermal source, and solar heat, into electricity[1]. In the past, solid-state materials have been applied for the thermoelectric conversion, e.g., inorganic materials[2], polymer matters[3], and organic–inorganic hybrid materials[4]. Recently, thermo-electrochemical (TEC) cells, which produce electric power using the temperature differences of an electrochemical cell containing a redox couple, have attracted considerable attention due to their high Seebeck coefficient (S_e) in the relatively low-temperature region. Electric potential is generated via the redox reaction described as:

$$A + ne^- \rightarrow B \tag{1}$$

with a S_e value expressed by[5,6]

$$S_e = \frac{\Delta V}{\Delta T} = \frac{S_B - S_A}{nF} \tag{2}$$

where V is the electric potential, T is temperature, S_A and S_B are the partial molar entropies of A and B, n is the number of electrons involved in the reaction, and F is the Faraday constant. High S_e values in the order of mV K^{-1} are achievable due to the large temperature dependence of equilibrium potentials for the reaction involving a multielectron redox reaction. Ferri/ferrocyanide ($Fe(CN)_6^{3-}/Fe(CN)_6^{4-}$), which has a S_e value of − 1.4 mV K^{-1} is one of the typical redox couples[7]. Moreover, various redox couples were investigated, e. g., iodide/triiodide(I^-/I_3^-)[8] and cobalt(II/III) tris(bipyridyl) ($Co^{2+/3+}$ $(bpy)_3$)[9] redox couple. The reported S_e value are listed in Table S1. Due to the increasing demand for the thermoelectric conversion, TEC cells with inexpensive and abundant materials are required. Until now, organic redox couples such as quinone/hydroquinone (quinhydrone)[10] and acetone/isopropanol[11] have been applied to TEC applications and large negative S_e values in organic redox couples system

[1]Department of Chemistry, Graduate School of Science, Kyushu University, Motooka 744, Nishi-ku, Fukuoka 819-0395, Japan. [2]Division of Applied Chemistry, Graduate School of Engineering, Kyushu University, Motooka 744, Nishi-ku, Fukuoka 819-0395, Japan. [3]Center for Molecular Systems, Kyushu University, Motooka 744, Nishi-ku, Fukuoka 819-0395, Japan. [4]Graduate School of Nanobioscience, Yokohama City University, Seto 22-2, Kanazawa-ku, Yokohama 236-0027, Japan. [5]Smart Innovation Program, Graduate School of Advanced Science and Engineering, Hiroshima University, Kagamiyama 1-4-1, Higashi-Hiroshima, Hiroshima 739-8527, Japan. [6]International Institute for Carbon-Neutral Energy Research (WPI-I2CNER), Kyushu University, Motooka 744, Nishi-ku, Fukuoka 819-0395, Japan. [7]Advanced Institute for Materials Research (WPI-AIMR), Tohoku University, 2-1-1 Katahira, Aoba-ku, Sendai 980-8577, Japan. ✉email: teppei@chem.s.u-tokyo.ac.jp; tishimo@hiroshima-u.ac.jp; yamauchi@i2cner.kyushu-u.ac.jp

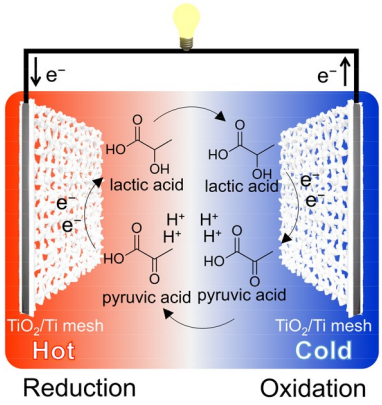

Figure 1. A scheme of thermo-electrochemical (TEC) cell using pyruvic acid and lactic acid as a redox couple and TiO_2/Ti mesh electrodes. Oxidation (or reduction) reaction proceeds at the cold (or hot) side.

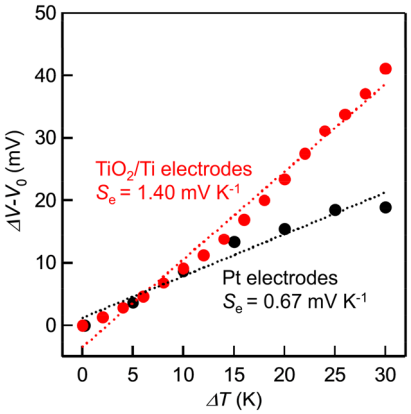

Figure 2. Difference in the open-circuit potential ($\Delta V - V_0$) and temperature difference (ΔT) of the TEC cell using TiO_2/Ti mesh electrodes (red) and Pt wire electrodes (black). V_0 is the initial open-circuit potential differences, as shown in Table S2. The initial concentration of pyruvic acid, lactic acid, and sodium sulfate were 20, 20 and 50 mM, respectively. Seebeck coefficients were calculated by the least-square fitting of a dotted line.

were obtained, e.g. – 0.63 to – 9.9 mV K^{-1}.[10,11] However, the carcinogenicity of quinhydrone or air sensitivity of isopropanol are drawbacks of these systems.

Considering the high efficiency of TEC cells in the low-temperature range, e.g., systemic temperatures, TEC conversion using body heat is a promising application[12]. In this regard, high biocompatible redox couples are needed, although few works for biocompatible couples have been performed. Herein, we focus on the TEC conversion using an organic redox couple composed of pyruvic acid and lactic acid. These compounds are ingredients in the metabolic system and intrinsically non-toxic. Recently, we have reported that α-keto acids are electrochemically reduced into corresponding α-hydroxyl acids on TiO_2 electrocatalyst with high efficiency[13–19]. In this report, we demonstrate TEC conversion employing a biocompatible redox couple of pyruvic acid and lactic acid, with the support of TiO_2 catalysts grown on a Ti mesh electrode (TiO_2/Ti mesh electrode)[15–19] as shown in Fig. 1. TEC cells were generally composed of expensive materials such as carbon nanotubes[20] and platinum.[21] Utilization of earth-abundant materials such as TiO_2 will accelerate the application of TEC cells.

Results and discussion

The TiO_2/Ti mesh electrode was prepared according to our previous report[15]. The XRD pattern shown in Fig. S1 represents that anatase type TiO_2 is contained in the electrode. The red plot in Fig. 2 and Fig. S2 show a difference in open-circuit potential ($\Delta V - V_0$) plotted to the temperature difference between two electrodes (ΔT) in the TEC cell, where V_0 is the initial open-circuit potential difference at $\Delta T = 0$. $\Delta V - V_0$ was calculated using the difference in the potential between two electrodes (Fig. S3). The larger ΔT resulted in the larger ΔV-V_0, which ensures conversion from heat energy to electrical power. We estimated the S_e value by the least square analysis of $\Delta V - V_0$ varying with ΔT (dashed line in Fig. 2) to be 1.40 mV K^{-1}, which is a positive S_e value. In contrast to the TEC conversion as shown in Fig. S4(a), the proportional relationship between $\Delta V - V_0$ and ΔT was not observed without pyruvic acid and lactic acid as indicated in Fig. S4(b). The deviation in the experiments without

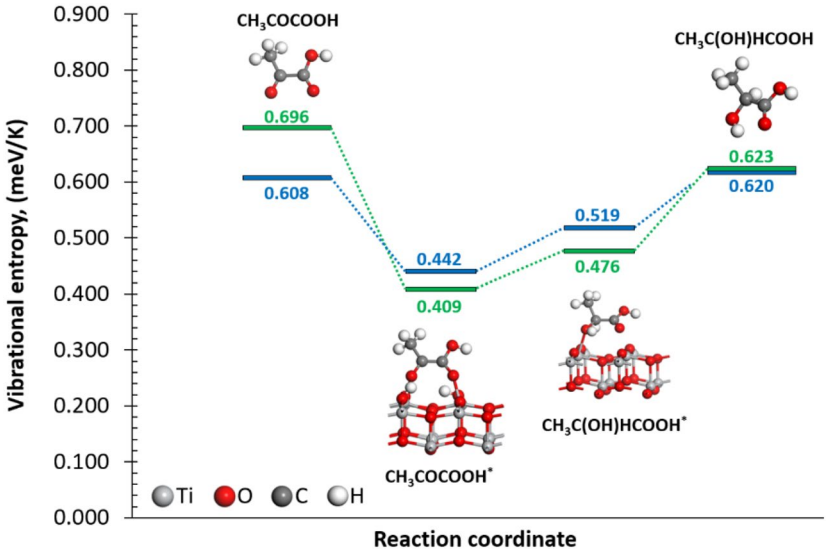

Figure 3. Vibrational entropies of the isolated and adsorbed pyruvic and lactic acid molecules. The green and blue paths correspond to the entropies without and with solvent effects, respectively.

the organic acids reflects the instability of the redox potential with the very low concentration of the redox molecules. The black plot in Fig. 2 displays $\Delta V - V_0$ plotted to ΔT of a TEC cell consisting of platinum electrodes. We observed a proportional relationship between $\Delta V - V_0$ and ΔT and determined the S_e to be 0.67 mV K^{-1}, which is less than one half of the S_e value for the cell using TiO_2/Ti mesh electrode, indicating catalytic natures of TiO_2 give positive effects on the TEC conversion.

Equation (2) represents that the electric potential change on electrodes resulting from the temperature difference is ascribed to entropy change in a common redox reaction. The redox reaction involving pyruvic acid and lactic acid is described as the following equation.

$$CH_3COCOOH + 2H^+ + 2e^- \rightleftharpoons CH_3C(OH)HCOOH \quad (3)$$

Equation (3) suggests that the entropy decreases along with the progress of the reduction of pyruvic acid. The standard Gibbs energies of formation for pyruvic acid and lactic acid are − 351.18 and − 314.49 kJ mol^{-1}[22], and standard enthalpies of formation for pyruvic acid and lactic acid are − 596.84 and − 687.88 kJ mol^{-1}, respectively[22]. From these thermodynamic parameters, the S_e value for the TEC system employing the redox reaction between pyruvic acid and lactic acid was estimated to be − 2.20 mV K^{-1}. This negative S_e leads to the progress of oxidation (or reduction) reaction at the hot (or cold) side, which is in contrast to the positive S_e value obtained in this system. Consequently, oxidation of lactic acid (or pyruvic acid reduction) proceeds at the cold (or hot) side in our TEC system. Previously, we recognized that the TEC cell with Pt electrodes resulted in the different S_e values from that with TiO_2/Ti electrodes, which suggests that the reaction mechanism depends on the materials used for the electrodes.

To investigate the reaction mechanism that shows the positive S_e value in this TEC system, density functional theory (DFT) calculations with solvent effect were performed and the reaction energy change between lactic acid and pyruvic acid on the TiO_2 surface was investigated. As a reaction field of pyruvic acid, the TiO_2(001) surface (Fig. S5) with two adsorbed H atoms is assumed. The thermodynamically stable interaction of two H atoms with two of the TiO_2(001) surface twofold coordinated O (O_{2c}) atoms leads to the formation of two OHs, as shown in Fig. S6a. Then the pyruvic acid reduction reaction is studied on the TiO_2(001) surface with the pre-adsorbed H atoms as an initial state. The most stable interaction of the pyruvic acid molecule on the protonated TiO_2(001) surface is the molecule with each of its uncoordinatedly saturated O atoms interacting with two surface Ti atoms closest to the already formed OHs. The relative energy of the adsorption of pyruvic acid on the protonated TiO_2 is − 0.816 eV. The reaction pathway of the pyruvic acid adsorption and its reduction to lactic acid by the sequential association of H atoms from the protonated TiO_2(001) surface is shown in Fig. S7. The first H association leading to the formation of $CH_3COHCOOH$ is an exothermic process with relative energy of − 0.846 eV. The association of the remaining H atom on the surface to the $CH_3COHCOOH$ leads to lactic acid formation. Compared to the first association, the second association is an endothermic process; the relative energy corresponding to the lactic acid formation is − 0.180 eV. The energy changes during the reaction were larger when the solvent effect is not considered, as shown in Fig. S7. Figure 3 shows the vibrational entropies of the isolated and adsorbed substrate molecules with and without solvent effects. The calculated vibrational entropies of the isolated pyruvic (0.608 meV K^{-1}) and lactic (0.620 meV K^{-1}) acids are larger than the values of the adsorbed molecules, 0.442 meV K^{-1} for the pyruvic acid and 0.519 meV K^{-1} for the lactic acid. The entropy difference between isolated and adsorbed molecules is just a reflection of the conversion of free translational/rotational/vibrational degrees of freedom into bound motions[23]. Based on these theoretical results, the positive relative energy, 0.636 eV, the oxidation of lactic acid is more energetically feasible than the pyruvic acid reduction.

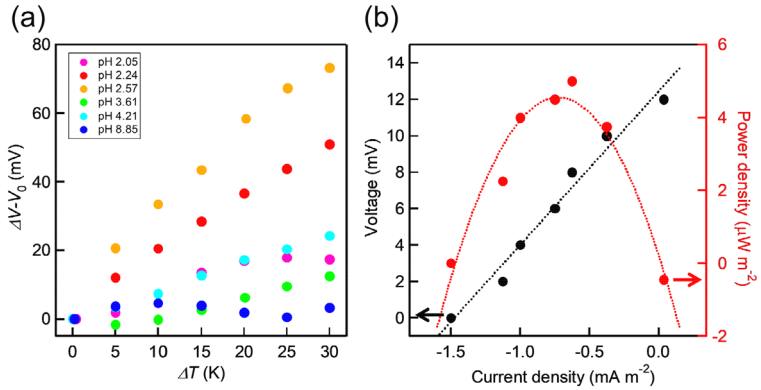

Figure 4. **(a)** pH dependence of $\Delta V - V_0$ and ΔT of the TEC cell. V_0 is the initial open-circuit potential difference, as shown in Table S2. The initial concentration of pyruvic acid, lactic acid, and sodium sulfate was 20, 20, and 50 mM, respectively. **(b)** Current output and the corresponding power output. The temperature difference was 10 K. (cold side at 291 K, hot side at 301 K). Dotted curves are inserted as an eye guide.

On the other hand, the vibrational entropy difference, 0.077 meV K^{-1}, between the adsorbed pyruvic and lactic acids was obviously positive, although isolated molecules are almost the same. Based on the vibrational entropy difference, the calculated S_e can be approximated to a value of 0.038 mV K^{-1}. The positive S_e value was obtained from the DFT calculations as well as from the experimental results. This result indicates that the existence of TiO_2 plays an essential part in showing a positive S_e sign. Additionally, one of the roles of the TiO_2 surface is the H donor/acceptor during the oxidation/reduction reactions. However, the large difference between the experimental and calculated S_e values remains. Although we found the importance of the solvent effect during the reaction. A reason for the discrepancy between theoretical and experimental results is that the solvent is treated as a structureless continuum with certain dielectric and interfacial properties.[24] In an explicit solvent model, the molecules can contribute over 90% of atoms in a simulated system, as a result, the number of interacting particles and the number of degrees of freedom of a system, and hence the entropy in the implicit models are significantly reduced.[25] Moreover, leaving out the explicit description of the solvent comes at the cost of lacking hydrogen bonds with solvent, overstabilized salt bridges, and hydrogen bonds within the solute, etc[25,26]. Other sources of discrepancy can be due to the homogeneity of the slab model considered in this work compared to the heterogeneity of the nanoparticles as the reaction might occur at ridge, vertex, or different facets. In the same line, the surface roughness, such as defects, is unclear for TiO_2 catalyst in our experiment. The presence of pre-adsorbed species, i.e., the coverage effect, also affects the change in entropy; for the carbolac-ethyl chloride system, at the start of the adsorption, there is an increase in entropy as the molecules are adsorbed in a disorderly array. In our calculation, we also found that when using TiO_2 surface without H adsorption, the calculated S_e value between adsorbed pyruvic and lactic acids is smaller, 0.027 mV K^{-1}. Then, as the surface becomes covered by a monolayer and the molecules are very orderly arranged, the entropy decreases. Finally, in the region of multilayer adsorption, there is a small entropy decrease that approaches zero. These three regions have been observed for the entropy changes in a variety of adsorption systems[27].

Figure 4a represents the pH-dependence of $\Delta V - V_0$. The slope of the lines increases with a decrease in pH values. At low pH conditions, a large number of protons interact with the TiO_2 surface and pyruvic acid molecules are associated with the protonated TiO_2 surface, according to the reaction pathway proposed in the DFT study (Fig. 3). In contrast, in the high pH region, the number of adsorbed protons possibly decreases and the H associations, which are illustrated in Fig. 3, hardly occur, resulting in a low S_e value. Thus, we conclude that the S_e value relates to the interaction between substrate molecules and the protonated TiO_2 surface.

The output power was evaluated from the *I-V* curve. Figure 4b reveals a relationship between current density (or power density) and the cell potential. ΔT between the electrodes was kept to be 10 K. A linear relationship was observed between the cell voltage and the current. The obtained power density was 5 μW m^{-2} in the TEC cell and smaller than the reported values for the other TEC cells[12]. To clarify the reason for the small power density, cell resistance was measured. The resistance of the cell was 0.015 MΩ, which is smaller than that estimated from the *I-V* plot (0.40 MΩ). Then, we attribute the small power density to the large resistance resulting from a high barrier for the transformation of redox species in our TEC cell and concentration polarization due to the smaller generation rate of pyruvic acid than that of lactic acid. Therefore, a large power density is probably achievable by optimizing electrolyte and cell design.

To evaluate the long-term stability, we continuously monitored current density and power density for 24 h, as shown in Fig S8. The power density gradually decreased for the first 2 h and then the constant value was maintained. The small power density is due to the slow oxidation reaction compared to that in cathodic side, according to the cyclic voltammogram shown in Figs. S9 and S10. The large power density will be maintained by the enhancement of the oxidation reaction.

The versatility of the redox species was also investigated. Fig. S11 shows the $\Delta V - V_0$ and ΔT between two electrodes in the TEC cell employing oxalic acid and glycolic acid as the redox couples. The $\Delta V - V_0$ increased

as the ΔT increased. Therefore, this result opens the perspective that various α-keto acids might be utilized as a redox couple for the TiO_2/Ti mesh electrode.

Conclusions

In summary, we first demonstrate the TEC conversion using a biocompatible organic redox couple, i.e., pyruvic and lactic acids, and the TiO_2/Ti mesh electrode with 1.40 mV K^{-1} of a positive S_e value. The DFT calculation revealed that the positive S_e value is ascribed to the difference in stability between lactic acid and pyruvic acid, which are adsorbed on the protonated TiO_2 surface. Furthermore, the TiO_2 surface acting as a proton donor (or acceptor) plays a critical role in determining the polarity of the generated potential. This result indicates that the interaction between redox species and electrode surface is considerably important in redox-based TEC conversion systems. Our findings suggest that favorable energy conversions will be achievable by designing redox couples and the electrode surface.

Experimental

Materials. Lactic acid, pyruvic acid, and glycolic acid were purchased from Tokyo Chemical Industry Co., Ltd. (TCI). Oxalic acid and sodium sulfate, anhydrous were purchased from Kishida Chemical Co., Ltd. Ti meshes (100 mesh) were provided by Manabe Industry Co., Ltd. All chemicals were used without purification.

Preparation of electrode. TiO_2/Ti meshes were prepared by two-step hydrothermal reactions that we reported previously[15]. 1 M NaOH solution was transferred to a 50 mL Teflon-lined stainless steel autoclave. Then titanium meshes (2×2.5 cm^2) were placed at Teflon-lined stainless steel autoclave. The hydrothermal treatment was conducted at 220 °C for 12 h. After the reaction, the autoclave was cooled to room temperature and the obtained titanate mesh was immersed in 0.1 M HCl solution for 10 min. Then, titanate mesh rinsed with deionized water. The deionized water was transferred to a 50 mL Teflon-lined stainless steel autoclave and titanate meshes were placed at Teflon-lined stainless steel autoclave. The hydrothermal treatment was conducted at 200 °C for 24 h. After the reaction, the autoclave was cooled to room temperature and the obtained TiO_2 meshes were rinsed with deionized water.

Characterization of electrode. X-ray diffraction (XRD) pattern was measured using Rigaku SmartLab diffractometer equipped with a Cu-Kα X-ray source ($\lambda = 1.5418$ Å).

Measurement for the open-circuit potential of TEC cells. A typical method of measurement for open-circuit potential is described below. As an electrolyte, lactic acid (20 mM), pyruvic acid (20 mM) were introduced into an H-shaped glass cell (Fig. S12 and sodium sulfate (50 mM) was added as a supporting electrolyte. The temperature of each branch was controlled by using a water bath. The solution was stirred by a magnetic stir bar. Two TiO_2/Ti mesh electrodes were separately soaked into the cell as shown in Fig. S12. The open-circuit voltage was measured as the potential difference between the two electrodes by Keithley 2401 source meter. The pH value of the solution was adjusted by introducing the aqueous solution of NaOH and/or sulfuric acid. The TiO_2/Ti mesh electrodes used for the measurement were put into pure water overnight with connected with the chips and wire before use.

Evaluation of long term stability. The long term stability was evaluated using an H-shaped glass cell. As an electrolyte, lactic acid (20 mM), pyruvic acid (20 mM), and sodium sulfate (50 mM) were introduced into the cell. The temperature of each branch was controlled by using a water bath. The hot side was kept at 306 K and the cold side was kept at 296 K. Two TiO_2/Ti mesh electrodes were separately soaked into the cell, and the voltage of 8 mV was applied by the VersaSTAT 3 potentiostat (Princeton Applied Research).

Cyclic voltammetry (CV) measurement. Cyclic voltammetry measurement was conducted using VersaSTAT 3 potentiostat (Princeton Applied Research) and a Teflon-caped glass cell. As an aqueous electrolyte, lactic acid (20 mM), pyruvic acid (20 mM), and sodium sulfate (50 mM) were introduced into the cell. TiO_2/Ti mesh, Ag/AgCl, and coiled Pt wire were soaked into the glass cell and used as working, reference, and counter electrodes, respectively. The current was recorded under a swept potential at a scan rate of 10 mV s^{-1}.

Computational details. All calculations performed in this study are based on the plane wave DFT method implemented in the Vienna Ab initio Simulation Package (VASP 5.4.4)[28–30]. Perdew – Burke – Ernzerhof parametrization under the generalized gradient approximation was employed as an exchange–correlation functional together with the projector augmented wave method[31]. Spin-polarized calculations were performed throughout the study with a plane wave cutoff energy of 500 eV. The convergence criteria for all calculations were set until the difference in total forces between two ionic steps was less than 0.02 eV/Å, and 10^{-5} eV/atom for the self-consistent field iterations. In this work, to correctly estimate the electronic properties of the Ti atoms, the GGA + U approximation with Hubbard parameter for Ti of 3.0 eV was selected, as it showed to fit the redox properties of TiO_2.[32] The optimization of the bulk TiO_2 anatase phase was performed with $15 \times 15 \times 6$ Monkhorst – Pack k-point mesh for the Brillouin zone integration where all the atoms and the crystal volume were allowed to relax. After the optimization, the calculated lattice parameters of bulk TiO_2 ($a = b = 3.882$ Å, and $c = 9.663$ Å), and the length of the Ti – O apical bond ($d = 2.008$ Å) are in good agreement with the experimental values ($a = b = 3.782$ Å, $c = 9.502$ Å, and $d = 1.979$ Å)[33]. Subsequently, the nine layers TiO_2(001) slab containing a total of 108 atoms was modeled. The TiO_2(001) surface was selected as it was suggested that the shape of the anatase

nanocrystallites is a truncated bipyramid exposing the (101) and (001) surfaces[34]. The slab was optimized with 3 × 3 × 1 Monkhorst – Pack k-point mesh. To avoid dipole – dipole interaction between the sides of the slab, the coordinates of the atoms in the middle three layers of the slab were kept frozen while the coordinates of the atoms in the three top layers for both sides of the slab were fully relaxed. The vacuum was set to span a range of 15 Å to ensure no significant interaction between the slabs, as shown in Fig. S5. To incorporate the effect of the presence of solvent, the self-consistent implicit solvation model incorporated in the VASPsol 2.0 software package was employed[35,36]. The dielectric constant of water was set to 75.70, which corresponds to the experimental dielectric constant at a temperature of 303 K.[37,38]The H atoms binding energy, E_{bind}, was defined as:

$$E_{bind} = E_{slab+H} - [E_{slab} + 2E_{H\ atom}] \tag{4}$$

where E_{slab+H}, E_{slab}, and $E_{H\ atom}$ are the total energies of the H atoms interacting with the TiO_2(001) surface, the pristine TiO_2(001) surface, and the isolated H atom, respectively. The two H atoms interaction leading to the formation of two OHs on the TiO_2(001) surface is thermodynamically favored with a binding energy of – 5.89 eV, and -5.86 eV when the solvent effect is considered. The pyruvic acid adsorption, E_{ads}, energy was calculated as follows:

$$E_{ads} = E_{slab+H+pyruvic} - [E_{slab+H} + E_{pyruvic}] \tag{5}$$

where $E_{slab+H+pyruvic}$, and $E_{pyruvic}$ are the total energies of the pyruvic acid molecule interacting with the protonated TiO_2(001) surface, and the isolated pyruvic acid molecule, respectively. The adsorption energy of the pyruvic acid on the protonated TiO_2(001) surface is – 1.33 eV and – 0.82 eV if the solvent effect is considered. The relative energy, E_{rel}, of the intermediates formed was calculated as follows:

$$E_{rel} = E_{int} - [E_{slab+H+pyruvic}] \tag{6}$$

where E_{int}, corresponds to the total energies of the reaction intermediates after the H atom association occurred. In all cases, a negative value of the binding, adsorption, and relative energies denotes a stable interaction. To assess the trend in stability change of the overall chemical reaction, the intermediate states were calculated without the transition state search.

Received: 2 September 2020; Accepted: 29 April 2021
Published online: 06 July 2021

References

1. Chu, S. & Majumdar, A. Opportunities and challenges for a sustainable energy future. *Nature* **488**, 294–303 (2012).
2. Taroni, P. J., Hoces, I., Stingelin, N., Heeney, M. & Bilotti, E. Thermoelectric materials: A brief historical survey from metal junctions and inorganic semiconductors to organic polymers. *Israel J. Chem.* **54**, 534–552 (2014).
3. Bubnova, O. *et al.* Optimization of the thermoelectric figure of merit in the conducting polymer poly(3,4-ethylenedioxythiophene). *Nat. Mater.* **10**, 429–433 (2011).
4. Toshima, N. Recent progress of organic and hybrid thermoelectric materials. *Synth. Met.* **225**, 3–21 (2017).
5. Quickenden, T. I. & Mua, Y. A review of power generation in aqueous thermogalvanic cells. *J. Electrochem. Soc.* **142**, 3985 (1995).
6. Dupont, M. F., MacFarlane, D. R. & Pringle, J. M. Thermo-electrochemical cells for waste heat harvesting – progress and perspectives. *Chem. Commun.* **53**, 6288–6302 (2017).
7. Hu, R. *et al.* Harvesting waste thermal energy using a carbon-nanotube-based thermo-electrochemical cell. *Nano Lett.* **10**(3), 838–846 (2010).
8. Abraham, T. J., MacFarlane, D. R. & Pringle, J. M. Seebeck coefficients in ionic liquids—Prospects for thermo-electrochemical cells. *Chem. Commun.* **47**, 6260–6262 (2011).
9. Abraham, T. J., MacFarlane, D. R. & Pringle, J. M. High Seebeck coefficient redox ionic liquid electrolytes for thermal energy harvesting. *Energy Environ. Sci.* **6**, 2639 (2013).
10. Midgley, D., Reference electrodes for use in the potentiometric determination of chloride. Part II. Quinhydrone electrodes *Analyst* **109**, 445–452 (1984).
11. Zhou, H. & Liu, P. High Seebeck coefficient electrochemical thermocells for efficient waste heat recovery. *ACS Appl. Energy Mater.* **1**, 1424–1428 (2018).
12. Duan, J. *et al.* Aqueous thermogalvanic cells with a high Seebeck coefficient for low-grade heat harvest. *Nat. Commun.* **9**, 1–8 (2018).
13. Watanabe, R., Yamauchi, M., Sadakiyo, M., Abe, R. & Takeguchi, T. CO_2-free electric power circulation via direct charge and discharge using the glycolic acid/oxalic acid redox couple. *Energy Environ. Sci.* **8**, 1456–1462 (2015).
14. Fukushima, T., Kitano, S., Hata, S. & Yamauchi, M. Carbon-neutral energy cycles using alcohols. *Sci. Technol. Adv. Mater.* **19**, 142–152 (2018).
15. Sadakiyo, M., Hata, S., Cui, X. & Yamauchi, M. Electrochemical production of glycolic acid from oxalic acid using a polymer electrolyte alcohol electrosynthesis cell containing a porous TiO_2 catalyst. *Sci. Rep.* **7**, 1–9 (2017).
16. Fukushima, T., Higashi, M., Kitano, S., Sugiyama, T. & Yamauchi, M. Multiscale design for high-performance glycolic acid electrosynthesis cell: Preparation of nanoscale-IrO_2-applied Ti anode and optimization of cell assembling. *Catal. Today* **351**, 12–20 (2020).
17. Sadakiyo, M., Hata, S., Fukushima, T., Juhász, G. & Yamauchi, M. Electrochemical hydrogenation of non-aromatic carboxylic acid derivatives as a sustainable synthesis process: From catalyst design to device construction. *Phys. Chem. Chem. Phys.* **21**, 5882–5889 (2019).
18. Fukushima, T. & Yamauchi, M. Electrosynthesis of amino acids from biomass-derivable acids on titanium dioxide. *Chem. Commun.* **55**, 14721–14727 (2019).
19. Fukushima, T. & Yamauchi, M. Electrosynthesis of glycine from bio-derivable oxalic acid. *J. Appl. Electrochem.* **51**, 99–106 (2021).
20. Hu, R. *et al.* Harvesting waste thermal energy using a carbon-nanotube-based thermo-electrochemical cell. *Nano Lett.* **10**, 838–846 (2010).
21. Quickenden, T. I. & Vernon, C. F. Thermogalvanic conversion of heat to electricity. *Sol. Energy* **36**, 63–72 (1986).
22. Alberty, R. A. Calculation of standard transformed Gibbs energies and standard transformed enthalpies of biochemical reactants. *Arch. Biochem. Biophys.* **353**, 116–130 (1998).

23. Ben-Tal, N., Honig, B., Bagdassarian, C. K. & Ben-Shaul, A. Association entropy in adsorption processes. *Biophys. J.* **79**, 1180–1187 (2000).
24. Ren, P. *et al.* Biomolecular electrostatics and solvation: A computational perspective. *Q. Rev. Biophys.* **45**, 427–491 (2012).
25. Zhang, J., Zhang, H., Wu, T., Wang, Q. & van der Spoel, D. Comparison of implicit and explicit solvent models for the calculation of solvation free energy in organic solvents. *J. Chem. Theory Comput.* **13**, 1034–1043 (2017).
26. Zhang, H., Tan, T. & van der Spoel, D. Generalized Born and explicit solvent models for free energy calculations in organic solvents: Cyclodextrin dimerization. *J. Chem. Theory Comput.* **11**, 5103–5113 (2015).
27. Pierce, C. & Smith, R. N. Heats of adsorption. IV. Entropy changes in adsorption. *J. Phys. Colloid Chem.* **54**, 795–803 (1950).
28. Kresse, G. & Hafner, J. *Ab initio* molecular dynamics for liquid metals. *Phys. Rev. B* **47**, 558–561 (1993).
29. Kresse, G. & Furthmüller, J. Efficient iterative schemes for *ab initio* total-energy calculations using a plane-wave basis set. *Phys. Rev. B* **54**, 11169–11186 (1996).
30. Kresse, G. & Furthmüller, J. Efficiency of ab-initio total energy calculations for metals and semiconductors using a plane-wave basis set. *Comput. Mater. Sci.* **6**, 15–50 (1996).
31. Blöchl, P. E. Projector augmented-wave method. *Phys. Rev. B* **50**, 17953–17979 (1994).
32. Hu, Z. & Metiu, H. Choice of *U* for DFT+*U* calculations for titanium oxides. *J. Phys. Chem. C* **115**, 5841–5845 (2011).
33. Burdett, J. K., Hughbanks, T., Miller, G. J., Richardson, J. W. Jr. & Smith, J. V. Structural-electronic relationships in inorganic solids: Powder neutron diffraction studies of the rutile and anatase polymorphs of titanium dioxide at 15 and 295 K. *J. Am. Chem. Soc.* **109**, 3639–3646 (1987).
34. Bourikas, K., Kordulis, C. & Lycourghiotis, A. Titanium dioxide (anatase and rutile): Surface chemistry, liquid–solid interface chemistry, and scientific synthesis of supported catalysts. *Chem. Rev.* **114**, 9754–9823 (2014).
35. Mathew, K., Sundararaman, R., Letchworth-Weaver, K., Arias, T. A. & Hennig, R. G. Implicit solvation model for density-functional study of nanocrystal surfaces and reaction pathways. *J. Chem. Phys.* **140**, 084106 (2014).
36. Mathew, K., Kolluru, V. S. C., Mula, S., Steinmann, S. N. & Hennig, R. G. Implicit self-consistent electrolyte model in plane-wave density-functional theory. *J. Chem. Phys.* **151**, 234101 (2019).
37. Moldoveanu, S. C. & David, V. Mobile phases and their properties. in *Essentials in Modern HPLC Separations* 363–447. https://doi.org/10.1016/B978-0-12-385013-3.00007-0 (Elsevier, 2013).
38. Owen, B. B., Miller, R. C., Milner, C. E. & Cogan, H. L. The dielectric constant of water as a function of temperature and pressure 1,2. *J. Phys. Chem.* **65**, 2065–2070 (1961).

Acknowledgements

We would like to show our special appreciation for the JSPS KAKENHI No. JP 18H05517, 19H05061 and 19H05062, (Hydrogenomics). We also thank JSPS grant number 17H03046 and JP19K22205, Joint Research by the National Institutes of Natural Sciences (NINS) Grant number 01112104 and JST-CREST, Japan. The computations were carried out using the computer resources offered under the category of General Projects by the Research Institute for Information Technology, Kyushu University.

Author contributions

H.E. and M.Y. wrote the main manuscript and T.K. and T.Y. constructed electrochemical sets and D.R. and T.I. conducted DFT calculations. All authors reviewed the manuscript.

Competing interests

The authors declare no competing interests.

Additional information

Supplementary Information The online version contains supplementary material available at https://doi.org/10.1038/s41598-021-93269-7.

Correspondence and requests for materials should be addressed to T.Y., T.I. or M.Y.

Reprints and permissions information is available at www.nature.com/reprints.

Publisher's note Springer Nature remains neutral with regard to jurisdictional claims in published maps and institutional affiliations.